Appendix J
WEST NEXRAD Analysis

Assessment of Nocturnal Bird Migration Activity from Weather Radar Data for the Proposed Icebreaker Wind Energy Facility, Lake Erie, Ohio

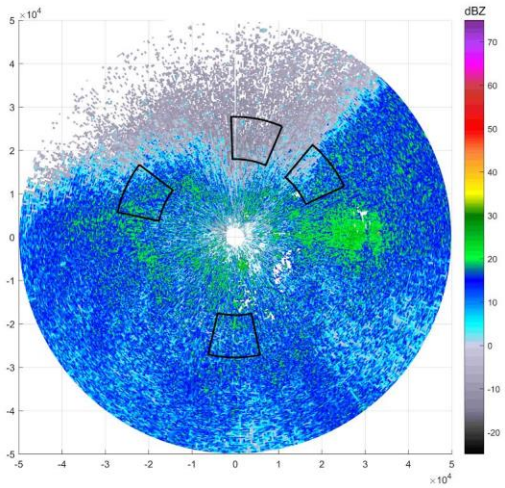

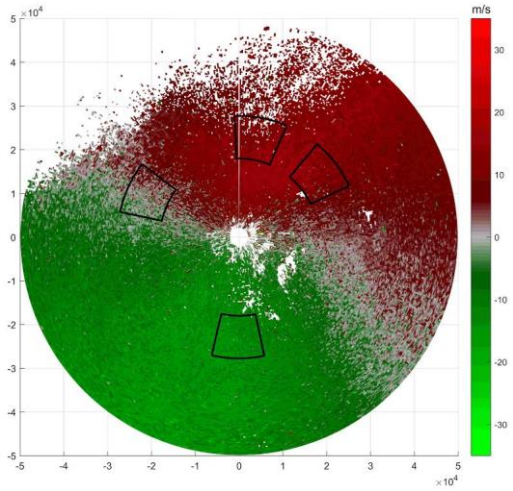

Prepared for:

Lake Erie Energy Development Corporation

1938 Euclid Avenue, Number 200
Cleveland, Ohio 44115

Prepared by:

Chris Nations and Caleb Gordon

Western EcoSystems Technology, Inc.
200 South Second Street
Laramie, Wyoming 82070

January 23, 2017

STUDY PARTICIPANTS

Western EcoSystems Technology

Caleb Gordon	Project Manager, co-author
Chris Nations	Statistician, lead author
Damian Stansbury	Data Technician
Janet Stansbury	Data Technician
Kristin Klaphake	GIS Technician
Jill Ottman	Technical Editor

TABLE OF CONTENTS

LIST OF TABLES

LIST OF FIGURES

INTRODUCTION

This study examines NEXRAD weather radar data from Cleveland, Ohio and another radar station in Buffalo, New York for the purpose of assessing nocturnal bird and bat migration above the proposed site of the Icebreaker Wind Energy Facility in Lake Erie, and several comparison areas near Cleveland and Buffalo. The acronym NEXRAD represents "NEXt generation RADar", a network of approximately 160 Doppler radar stations maintained by the National Weather Service, and designed to monitor precipitation throughout the United States. NEXRAD data are stored and disseminated in two forms–as raw, high resolution Level II data, and as more highly processed, lower resolution Level III data. Level II products include reflectivity (a measure of the density of reflecting targets), radial velocity (the component of velocity either toward or away from the radar unit), and several other products (NOAA 2016). Most radar ornithological studies published to date have relied on analysis of reflectivity and radial velocity (e.g., Diehl et al. 2003, Gauthreaux and Belser 2003, Bonter et al. 2008, Buler and Dawson 2014, Farnsworth et al. 2016).

During operation, a radar unit sweeps horizontally through 360 degrees at each of several elevation angles (usually including 0.5°, 1.5°, 2.5°, 3.5°, and 4.5°) (NOAA 2016). The half-power beam width is approximately 0.95 degrees (Raghavan 2013), though energy return is greatest in the center of that beam. As of 2008, so-called "super resolution" Level II data for the lowest two elevations (0.5 degrees and 1.5 degrees) available from most NEXRAD stations have azimuthal resolution of 0.5 degrees and range resolution of 250 m (Torres and Curtis 2007). Thus, returned energy represents all targets within a section of a cone with 0.5 degrees "width" and "depth" of 250 m. Because of beam spread, the volume of this cone section increases with increasing range. From an analysis standpoint, the cone section represents the most fundamental sample unit for NEXRAD data. In the Methods section below, these cone sections are referred to as "pixels" of the polar coordinate system defined by radar azimuth and range.

Analysis of NEXRAD data for ornithological research depends on separating targets that are most likely to be birds (and/or bats) from other radar targets (Gauthreaux and Belser 1998). This data filtering process operates on the assumption that birds can fly opposing the wind or, if flying in the same direction as the wind, they can fly at greater than wind speed. Other targets will move with the wind (e.g., light precipitation or airborne dust) or only slightly faster than the wind (e.g., large swarms of insects). Thus, filtering out the slower-moving targets relies on independent measurements of wind speed and direction. Radiosonde wind data are obtained from weather balloons that are launched regularly from 92 stations in North America and the Pacific Islands (http://www.ua.nws.noaa.gov/). Many, though not all, radiosonde locations are coincident with NEXRAD stations. Data collected by instruments suspended from the balloon are radioed back to the station on the ground. At stations without radiosonde operations, winds at altitude must be estimated by other means, for example, from ground-based measurements (e.g., Archibald et al. 2016) or atmospheric wind models (e.g., Livingston 2008).

METHODS

Project Site, NEXRAD Stations, and Radar Sample Areas

The proposed Icebreaker Wind Facility will consist of six turbines (with a seventh alternate) in a single row, located approximately 14 km (9 miles) from the nearest point on the Lake Erie shoreline and 23 km (14 miles) from the KCLE NEXRAD station in Cleveland, Ohio (Figure 1). For the purpose of creating a reasonably sized sample area above the project, first, a boundary was defined as the 3.2 km (2 mile) buffer around the line segment connecting the turbines. The buffer was a racetrack-shaped polygon that provided range and azimuth limits for a NEXRAD sample area (Figure 2a), hereafter referred to as the Project Area. The Project Area was a wedge-shaped polygon with minimum range of 18 km, maximum range of 27.75 km, and arc limits spanning 25 degrees. Given the radar resolution for range (250 m) and azimuth (0.5°), the Project Area covered 39 range gates and 50 radar azimuths, or a total of 1950 pixels (= 39 × 50). The entire Project Area was above water (Figure 2a). Several comparison areas were created with the same size, range limits, and arc length as the Project Area. By design, these areas sampled air spaces at the same ranges so that, for fixed target sizes and densities within

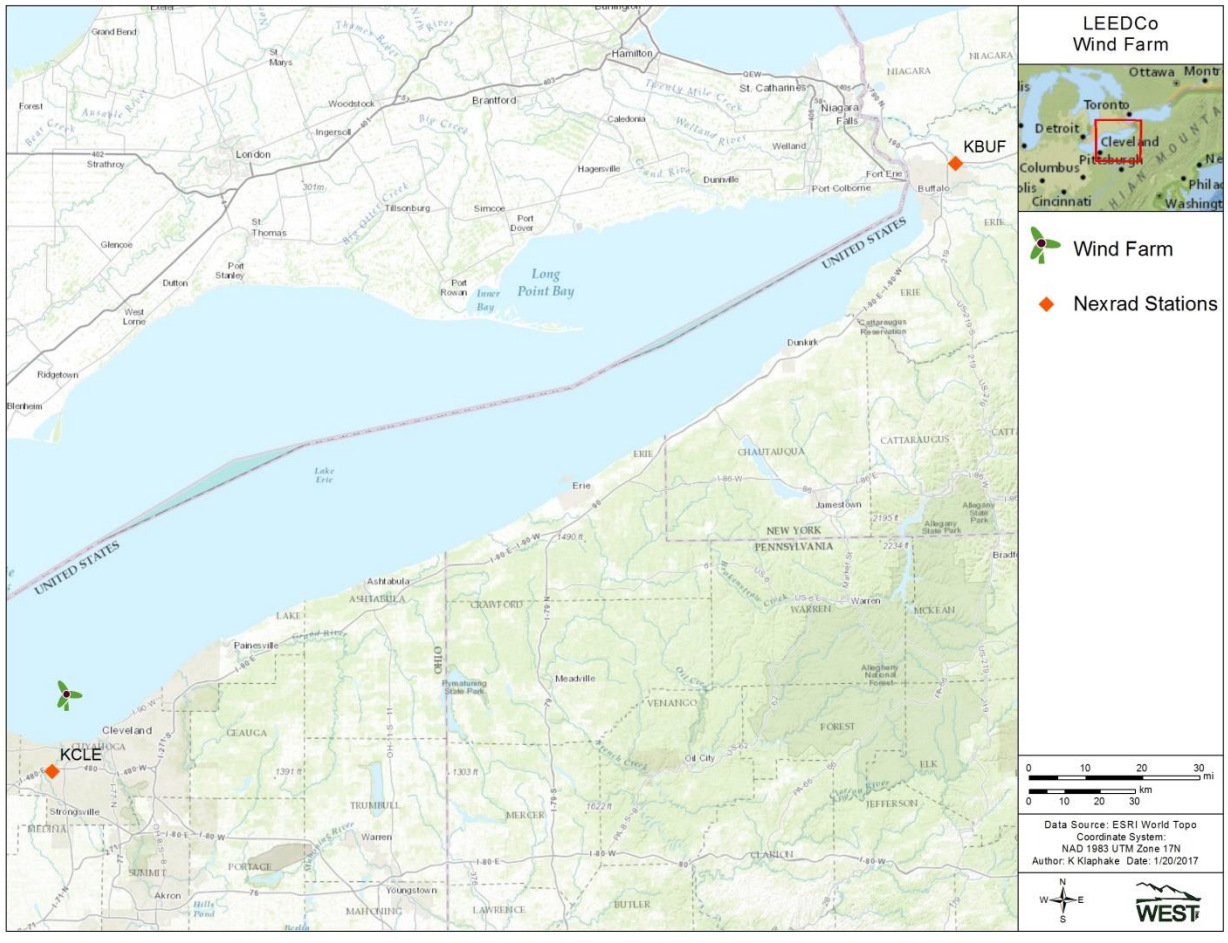

Figure 1. Location of the proposed Icebreaker Wind Energy Facility in Lake Erie, in relation to the KCLE NEXRAD station in Cleveland, OH and the KBUF station in Buffalo, NY.

(a)

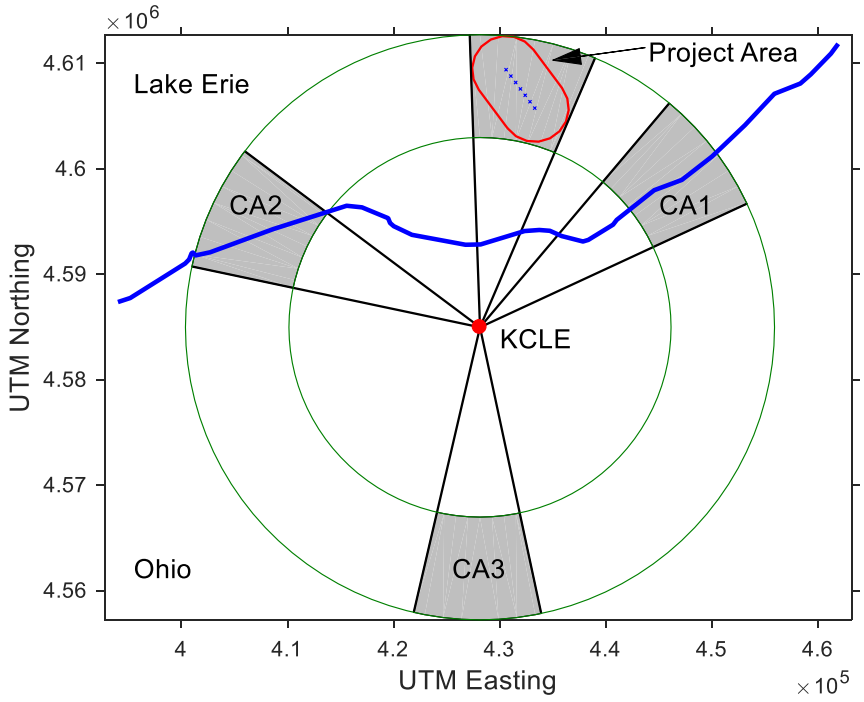

(b)

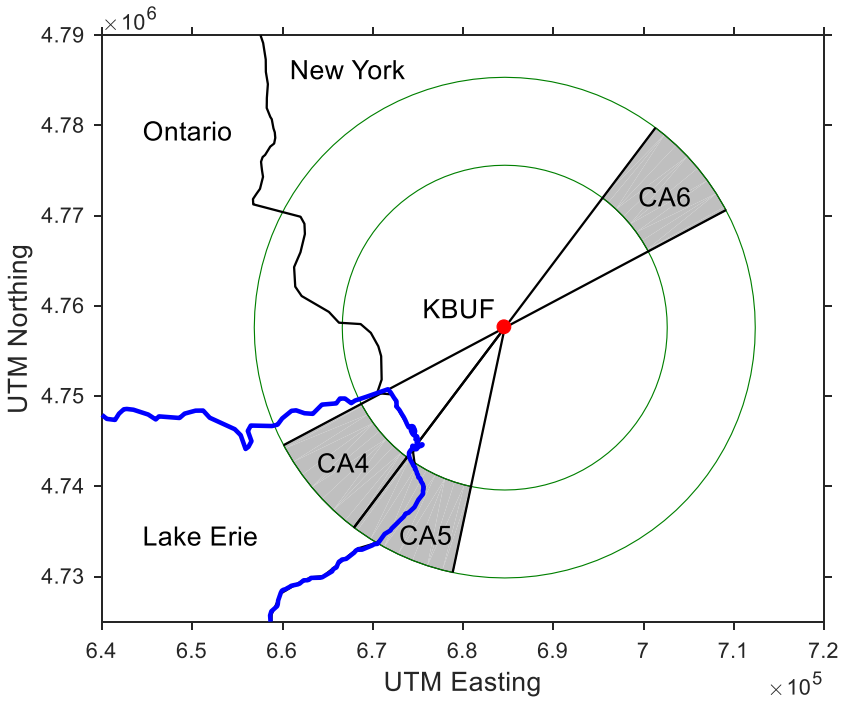

Figure 2. NEXRAD stations (red circles) and sample areas (gray shading), all at the same ranges (green circles) with same arc length (25 degrees) as the Project Area at (a) Cleveland (KCLE) and (b) Buffalo (KBUF). The Project Area in (a) shows the wind turbine locations (small blue circles) for the proposed Icebreaker Wind Energy Facility and bounding polygon (red line) used to define sample area dimensions.

each space, return energy would not differ. Furthermore, these areas sampled the same altitudes relative to the NEXRAD stations (though, altitude relative to ground or lake surface would vary somewhat). Three comparison areas were defined for KCLE (Figure 2). Comparison Areas 1 and 2 were situated above the Lake Erie shoreline such that approximately half of each area was above water and half was above land. Comparison Area 3 was located to the south of KCLE, entirely above land. Similarly, three comparison areas were defined for KBUF (Figure 2b). Comparison Area 4 was situated to the southwest of KBUF, entirely above water, though closer to the lake shore than the Project Area at KCLE. Comparison Area 5 was adjacent to Comparison Area 4, situated partly above water and partly above land, and Comparison Area 6 was entirely above land to the northeast of KBUF.

As described in the next section, only data from the lowest two radar elevations (0.5 degrees and 1.5 degrees) were retained for analysis. The height of the radar beam above the lake surface at the Project Area (i.e., the sample area shown in Figure 2a) was calculated accounting for radar height, earth curvature, and atmospheric refraction (Doviak and Zrnic 2006). In particular, beam height, *H*, was calculated as:

$$H = \sqrt{d^2 + \left(\frac{4}{3}r\right)^2 + 2d\frac{4}{3}r\sin(\theta)} + h_a - \frac{4}{3}r$$

where *d* = radar range (distance from the radar unit to the point of interest on the earth's surface), *r* = earth radius, θ = radar elevation, and h_a = height of the radar antenna relative to the point of interest. In addition to height of the beam center, the heights of the −3 dB (half-power) points were also calculated. As shown in Figure 3, the height of the center of the radar beam above the Project Area ranged from 257 to 366 m at the 0.5 degree elevation and from 574 to 847 m at the 1.5 degree elevation. Figure 3 also shows that at the 0.5 degree elevation the height of the lower −3 dB point ranged from 105 to 135 m above the Project Area. Thus, there was some overlap of the radar beam and the rotor-swept zone for the proposed turbines, which have a maximum blade tip height of 146 m. Figure 3 shows the area occupied by turbines (based on the proposed locations and height) as a semi-transparent gray rectangle, thus illustrating the overlap region. Table 1 provides more detail about radar beam height directly above the turbine locations. Note, for instance, that the lower −3 dB point ranged from 114.4 to 124.6 m directly above the turbine locations. Birds flying within the overlap region would likely be detected by the KCLE NEXRAD, though more detailed inference about target heights is not possible. Chilson et al. (2012) maintain that because birds are "bright" targets (relative to precipitation), a more appropriate characterization of beam width would be based on the −6 dB (quarter-power) points. That wider beam would imply greater overlap with the rotor-swept zone within the Project Area, i.e., detection of birds at lower heights (as well as at greater heights).

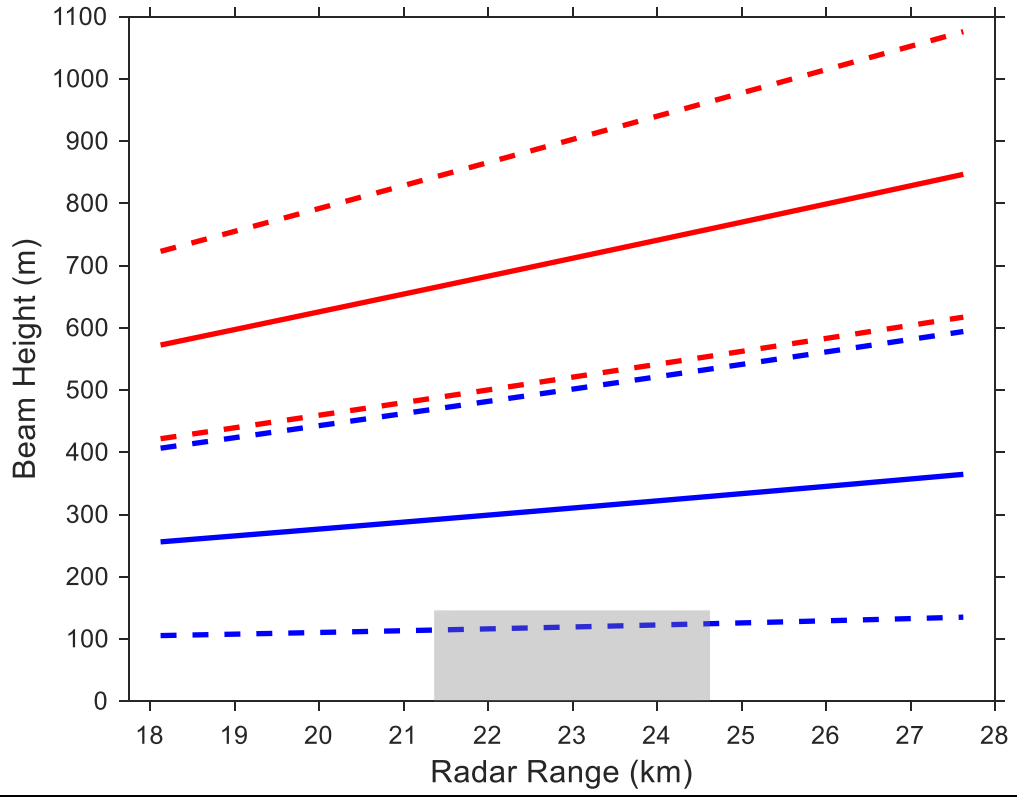

Figure 3. NEXRAD beam height relative to the lake surface, above the Project Area (X-axis limits) and, more specifically, above the wind turbines (gray shading). Solid lines indicate the beam centers, and dotted lines represent approximate beam boundaries of the 0.5^0 (blue) and 1.5^0 azimuth radar beams.

Table 1. Sampling heights of the radar beam from the KCLE station above the proposed Icebreaker Wind Energy Facility.

Radar Elevation	Position Within Beam	Beam Height (m) Near (21.36 km)	Far (24.63 km)
0.5°	Lower	114.4	124.6
	Center	291.9	329.2
	Upper	469.3	533.7
1.5°	Lower	487.2	554.4
	Center	664.6	758.9
	Upper	842.0	963.4

Heights are given for the nearest and farthest wind turbines from KCLE. “Lower” and “Upper” positions within the beam refer to the −3 dB (half-power) points for beam width of 0.95°. Beam heights account for land elevation and tower height at the KCLE site relative to the lake surface.

Data Selection, Downloading, and Pre-Processing

Level II NEXRAD data were downloaded from the database maintained by the National Centers for Environmental Information (NCEI) archival website (https://www.ncdc.noaa.gov/has/has.dsselect). Data were obtained from both the primary radar station (KCLE at Cleveland, OH) and the comparison station (KBUF at Buffalo, New York) for the nighttime hours during the spring and fall migratory periods, defined as April 1 – May 31 and August 20 – October 20, respectively. Fall data were obtained for the three years 2013 – 2015, and spring data were obtained for the years 2014 – 2016. While Fall 2016 data were available from KCLE, comparable data for the same period were not available from KBUF.

Each downloaded compressed file containing all data for an hour was decompressed into multiple files, each representing a separate radar scan at multiple elevations; typically, weather radars conduct 5 – 10 scans per hour. The NEXRAD data in these decompressed files were extracted from the native binary format using the Weather and Climate Toolkit, a Java program obtained from the NCEI (http://www.ncdc.noaa.gov/wct/). The Toolkit was used to export each file into NetCDF (Network Common Data Form) format (http://www.unidata.ucar.edu/software/netcdf/). NetCDF is a scientific data format that is machine independent and is readily imported by a variety of analysis software. Each NetCDF file contained all data from the native NEXRAD file in the original polar coordinate system (radar azimuth and range). NetCDF files were queried using Matlab, and only those files representing NEXRAD operation in Clear Air Mode (Volume Coverage Patterns 31 or 32) were retained for further processing and analysis. Files representing operation in Precipitation Mode, i.e., not in Clear Air Mode, were assumed to be dominated by precipitation and thus have little, if any, interpretable data indicative of bird migration. Other studies have excluded data due to precipitation (e.g., Farnsworth et al. 2016). Furthermore, Precipitation Mode data have lower resolution than data from Clear Air Mode, making analysis of biological targets more difficult (Diehl and Larkin 2005). Files were further filtered to retain only radar scans occurring between civil sunset (30 minutes after sunset) and civil sunrise (30 minutes before the following sunrise). This temporal filtering focused on the nocturnal period when migration is most intense (Diehl and Larkin 2005, Farnsworth et al. 2016), and also minimized contamination of scans due to sun strobes, which tend to occur near sunset and sunrise (Gauthreaux and Belser 2003).

All remaining NetCDF files were imported into Matlab and subset to retain “Super Resolution” reflectivity and radial velocity at 0.5 degree and 1.5 degree elevations; that is, all other Level II products and all higher elevations were discarded. Furthermore, data were subset to retain ranges less than 50 km. These subsetting steps led to greatly reduced file sizes and thus subsequently facilitated faster data processing and analysis. At the same time, 50 km range included substantial area beyond the Project site and similar comparison areas (described below) to facilitate visual pre-screening of radar scans.

Radar data were visually pre-screened in two stages to identify problems in radar scans. In the first stage, a technician viewed each scan at each elevation, displayed as a reflectivity-velocity pair, and flagged scans with potential problems such as precipitation (light precipitation may occur in Clear Air Mode), radar malfunction, or other anomalies. In the second stage, a more

experienced person viewed those scans that had been flagged, and made a final determination regarding data acceptability. In particular, each sample area within each of the provisionally flagged scans was given a final flag if it was considered unacceptable, for example, because precipitation occurred within that area. In many cases, only one or two sample areas were flagged, while the remaining sample areas were considered acceptable. Flagged sample areas were not included in subsequent analysis. Other than pre-screening as described, all data were retained without regard to intensity of presumed migration (reflectivity values) or direction (inferred from radial velocity images); that is, there was no attempt made to pre-select occurrences of pronounced bird migration.

Target Filtering

Identification of likely bird migration required separation of targets based on estimated air speeds under the assumption that targets with relatively high air speed were birds (or bats) and those with air speeds closer to the wind were either completely passive (e.g., dust, smoke, or light precipitation) or weak fliers such as insects. An air speed threshold of 5 m/s (Buler and Dawson 2014) was used to separate these two target classes; i.e., targets with air speed greater than 5 m/s were interpreted as birds. Calculation of air speed required estimates of both target ground speed and wind speed. Target ground speeds were calculated from NEXRAD radial velocities, while wind speeds were based on vertical wind profiles from either radiosonde or modeled wind data.

NEXRAD radial velocity data does not provide a direct estimate of target ground velocity, except in those cases when targets are moving directly towards or away from the radar station. Under the assumption that target speed and direction are uniform across broad areas (typically, though not necessarily, at 360 degrees around the radar unit), they can be estimated using the "wind retrieval" techniques developed by meteorologists. The Velocity Azimuth Display (VAD) algorithm (Browning and Wexler 1968) provides one such approach. Regression is generally used to estimate mean velocities and also yields estimates of variability in radial velocity, though it is computationally intensive when radar scans number in hundreds to thousands. Liang and Wang (2009) describe a VAD technique that is simpler than regression, though it does not yield any estimate of variance.

Target ground velocity was calculated following Liang and Wang (2009) with the assumption that velocity was uniform around the circle at a given radar range (thus, uniform at a given height), but potentially varying at different ranges (heights). Letting θ_i represent radar azimuth (i = 1, …, 720), $V_{\theta_{i,j}}$ represent radial velocity at the i^{th} azimuth and the j^{th} range (j = 1, …, 39, for ranges within the sample areas), then the east-west and north-south velocity components at the j^{th} range were calculated, respectively, as:

$$u_j = \frac{-\sum_i V_{\theta_{i,j}} \cos(\theta_i)}{\sum_i \cos^2(\theta_i)}$$

$$v_j = \frac{-\sum_i V_{\theta_{i,j}} \sin(\theta_i)}{\sum_i \sin^2(\theta_i)}$$

Then, ground speed, $V_{j,g}$, and direction, $\phi_{j,g}$, were recovered, respectively, as:

$$V_{j,g} = \sqrt{u_j^2 + v_j^2}$$

$$\phi_{j,g} = \tan^{-1}(v_j/u_j)$$

In addition to their use in calculating target air speeds (see below), calculated ground directions were retained for subsequent analysis of migration direction.

Radiosonde data including wind speed and direction were obtained for KBUF from a website maintained by the University of Wyoming Department of Atmospheric Science (http://weather.uwyo.edu/upperair/sounding.html). These data were available at 12-hour intervals (at 00:00 and 12:00 UTC). For KCLE, no radiosonde data were available, so modeled vertical profile wind data were obtained from the Earth Systems Research Laboratory (ESRL, part of the National Oceanic and Atmospheric Administration) (http://www.esrl.noaa.gov/ psd/map/profile/). The modeled R1 Reanalysis data from ESRL are based on radiosonde and other measurements, and are available on a global 2.5 degree grid (latitude and longitude) at 6-hour intervals (00:00, 06:00, 12:00, and 18:00 UTC). For KCLE at 41.41° north, 81.86° west, the nearest model grid point was 42.50° north, 82.50° west.

Two-dimensional linear interpolation of vertical profile wind (whether radiosonde or modeled) was performed to estimate wind speed and direction across (1) time, to match the times at which radar scans were conducted, and (2) height, to match the calculated height of the radar beam at each range value within the sample areas. Interpolation was conducted separately for each night of radar data. Given the relatively coarse temporal resolution of the wind data, there were typically two to four sets of wind data spanning each night (before, during, and after the night's radar scans). Similarly, given the height resolution of the wind data and the relatively low heights of the radar beam within the sample areas, there were at most six height observations in each modeled wind dataset and at most 30 height observations in each radiosonde dataset. Interpolation was conducted for all radar beam heights within the sample areas at both the 0.5 degree and 1.5 degree radar beam elevations. Wind speed was interpolated directly. For wind direction, the cosine and sine transformations were calculated first, each transform was separately interpolated across time and height, and then directions were recovered as the arctangent transformation of the two components. Aside from the trigonometric transformations for direction, linear interpolation was not substantially more complicated than nearest-neighbor interpolation since both required calculation of numerous differences in both time and height.

Representing wind speed and direction at the j^{th} range (height) as $V_{j,w}$ and $\phi_{j,w}$, respectively, air speed, $V_{j,a}$ was calculated as:

$$V_{j,a} = \sqrt{V_{j,g}^2 + V_{j,w}^2 - 2V_{j,g}V_{j,w}\cos(\phi_{j,g} - \phi_{j,w})}$$

If target air speed at the j^{th} range was less than 5 m/s, then the corresponding reflectivity values within each sample area were set to missing values, i.e., those reflectivity values were excluded

from further analysis. Otherwise, if target air speed exceeded 5 m/s, reflectivity values at that range were considered to be migrating birds and were retained for analysis.

In a final filtering step, each radar scan was evaluated and the data within each sample area were retained for analysis if at least 20 percent of the pixels had non-missing reflectivity values. Thus, certain sample areas within a scan might have been eliminated while the remaining sample areas from that scan were retained.

For subsequent analysis, reflectivity values were transformed from the logarithmic (*dBZ*) to the linear (*Z*) domain using the relationship:

$$Z = 10^{dBZ/10}$$

as in Diehl et al. (2003).

Analysis

Before any further processing, target direction data were averaged for each radar scan, at each beam elevation. Given the limited spatial resolution of both the VAD "wind retrieval" technique and the vertical profile wind data (whether from radiosonde or wind model), calculated target direction was the same for all sample areas at each radar station, though it might vary somewhat with beam elevation. Because direction is a circular variable, average direction, $\bar{\phi}$, was calculated as

$$\bar{\phi} = tan^{-1}(Y/X), \text{ where}$$

$$X = \sum_{i=1}^{n} \cos(\phi_i)/n \quad \text{and} \quad Y = \sum_{i=1}^{n} \sin(\phi_i)/n$$

where ϕ_i was the direction at range *i* (Batschelet, 1981). On the other hand, target reflectivity data were averaged separately for each sample area, at each radar elevation within each scan. That is, each sample area was represented by a single mean reflectivity value (for each scan and elevation); those mean values were treated as the observations in subsequent data summaries.

Target Direction

Summaries of target direction included the mean (calculated as above) by station, season, and elevation, or by station, season, year, and elevation. In addition, summaries included angular concentration, *r*, and standard deviation, *s*. Angular concentration (Batschelet, 1981) was calculated as

$$r = \sqrt{X^2 + Y^2}$$

where *X* and *Y* were the averages of the cosine and sine components of direction, respectively, as above. Angular concentration can vary between 0 (low concentration) and 1 (high concentration), with 0 occurring if directions are uniformly distributed on the circle, and 1 occurring if all directions are coincident. Angular standard deviation (Mardia 1972) was calculated as

$$s = \sqrt{-2\log_e(r)}$$

Ninety-five percent confidence intervals for mean direction were calculated using bootstrapping (Manly 2006). In particular, 1000 bootstrap samples were taken in which the data were sampled with replacement, the mean direction was calculated for each sample, and the lower and upper 95% confidence limits were calculated as the 2.5th and 97.5th percentiles, respectively.

Target Density

Radar reflectivity representing target density was averaged in various ways to make comparisons between sample areas or radar stations, by radar elevation, hour of the night, date, season, or year. In all cases, means and standard errors were calculated for graphical presentation. Serial correlation in reflectivity was not assessed, nor were standard errors corrected for such correlation. Reflectivity was not converted to bird density since such conversion is based on the important assumptions that target size is known and is uniform (Chilson and Adams 2014). Furthermore, conversion does not facilitate comparisons within this study.

RESULTS

After eliminating radar scans due to precipitation or other problems, 24,029 scans remained for analysis. In this case, a single scan refers to the data collected at both the 0.5 degree and 1.5 degree elevations, and a scan would have been retained for analysis if there were useable data in at least one of the sample areas at one elevation, though for most scans, there was useable data in all sample areas at both elevations. There were roughly equal numbers of scans at the two stations, 12,285 at KCLE and 11,744 at KBUF (Table 2). However, number of scans differed by season: 9,857 in the spring, and 14,172 in the fall. In part, the smaller number of scans in the spring was due to shorter nighttime periods in that season. Table 3 summarizes the number of scans with useable data by sample area and radar elevation as well as season and year. For instance, for the Project Area, in spring 2014, there were 1,525 scans at the 0.5 degree elevation and 1,458 scans at the 1.5 degree elevation.

Table 2. Number of radar scans by station, season, and year

Season	Year	KCLE	KBUF	Total
Spring	2014	1834	1974	
	2015	1551	1720	
	2016	1798	980	
	Total	**5183**	**4674**	**9857**
Fall	2013	2364	2323	
	2014	2235	2075	
	2015	2503	2672	
	Total	**7102**	**7070**	**14172**
Total		**12285**	**11744**	**24029**

Table 3. Number of scans with useable data by sample area, season, year, and radar elevation. Sample areas are designated as in Figure 2: PA = Project Area; CA = Comparison Area.

Season	Year	Elevation	KCLE				KBUF		
			PA	CA1	CA2	CA3	CA4	CA5	CA6
Spring	2014	0.5°	1525	1573	1558	1573	1667	1816	1688
		1.5°	1458	1614	1610	1638	1378	1429	1300
	2015	0.5°	1180	1344	1305	1337	1496	1542	1516
		1.5°	1075	1246	1189	1262	1414	1475	1451
	2016	0.5°	1433	1499	1490	1517	696	876	706
		1.5°	1378	1540	1510	1516	535	634	533
Fall	2013	0.5°	1980	1989	1989	1991	1615	1601	1617
		1.5°	1907	1983	1942	1989	1936	1932	1936
	2014	0.5°	2120	2122	2127	2126	1683	1668	1677
		1.5°	2090	2137	2127	2140	1821	1809	1817
	2015	0.5°	2161	2163	2163	2172	2514	2525	2511
		1.5°	2123	2139	2150	2156	2563	2575	2543

Migration Direction

Target directions are summarized in Figures 4 and 5, and Table 4. Rose plots show the distribution of all direction data by season and radar elevation for KCLE (Figure 4) and KBUF (Figure 5). The corresponding mean directions and associated 95 percent confidence limits are shown by red lines on each plot. In general, target directions were consistent with expected seasonal migration patterns. In the fall, target directions were toward the southwest at KCLE (Figure 4a, c) and toward the south or south-southeast at KBUF (Figure 5a, c). In the spring, target directions were predominantly toward the north-northeast at both stations (Figures 4b, 4d, 5b, 5d). In terms of general patterns and means, target directions were similar at both radar elevations within seasons at each station. However, at KBUF in the fall, mean fall directions did differ somewhat between the two radar elevations. In all cases, there was substantial variation in direction; most of the rose plots show that at KCLE there were targets moving in all directions, irrespective of season and radar elevation. At KBUF, the patterns were more complicated. For instance, in the fall, there were very few targets with northerly headings between 270 degrees and 45 degrees, but otherwise, headings showed fairly wide dispersion (Figure 5a, c).

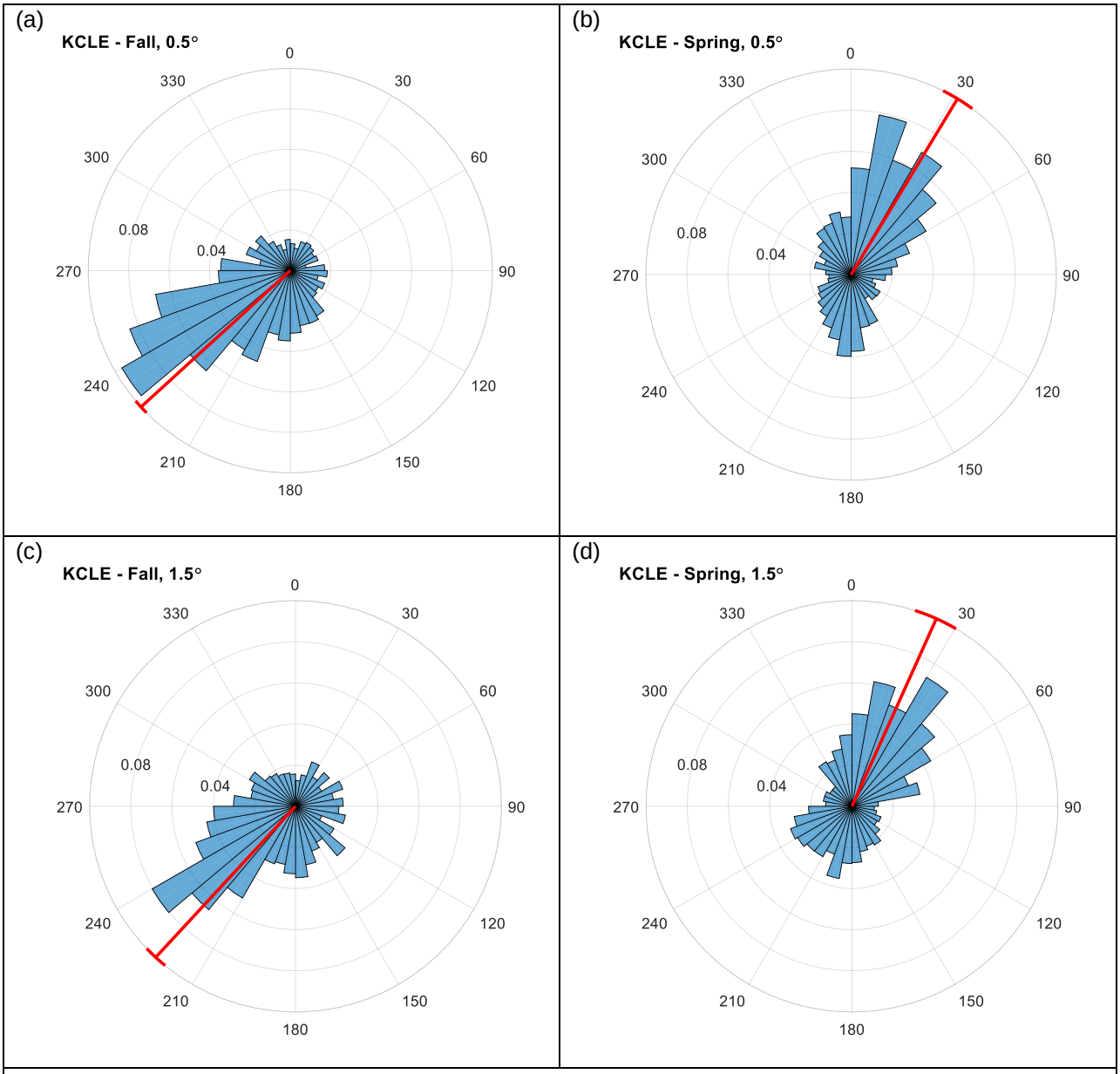

Figure 4. Rose plots showing target movement directions at KCLE at radar beam elevations of 0.5° (a and b) and 1.5° (c and d) in Fall (a and c) and Spring (b and d). Red lines indicate mean direction (radial segment) and 95% confidence interval (perpendicular "T" segment).

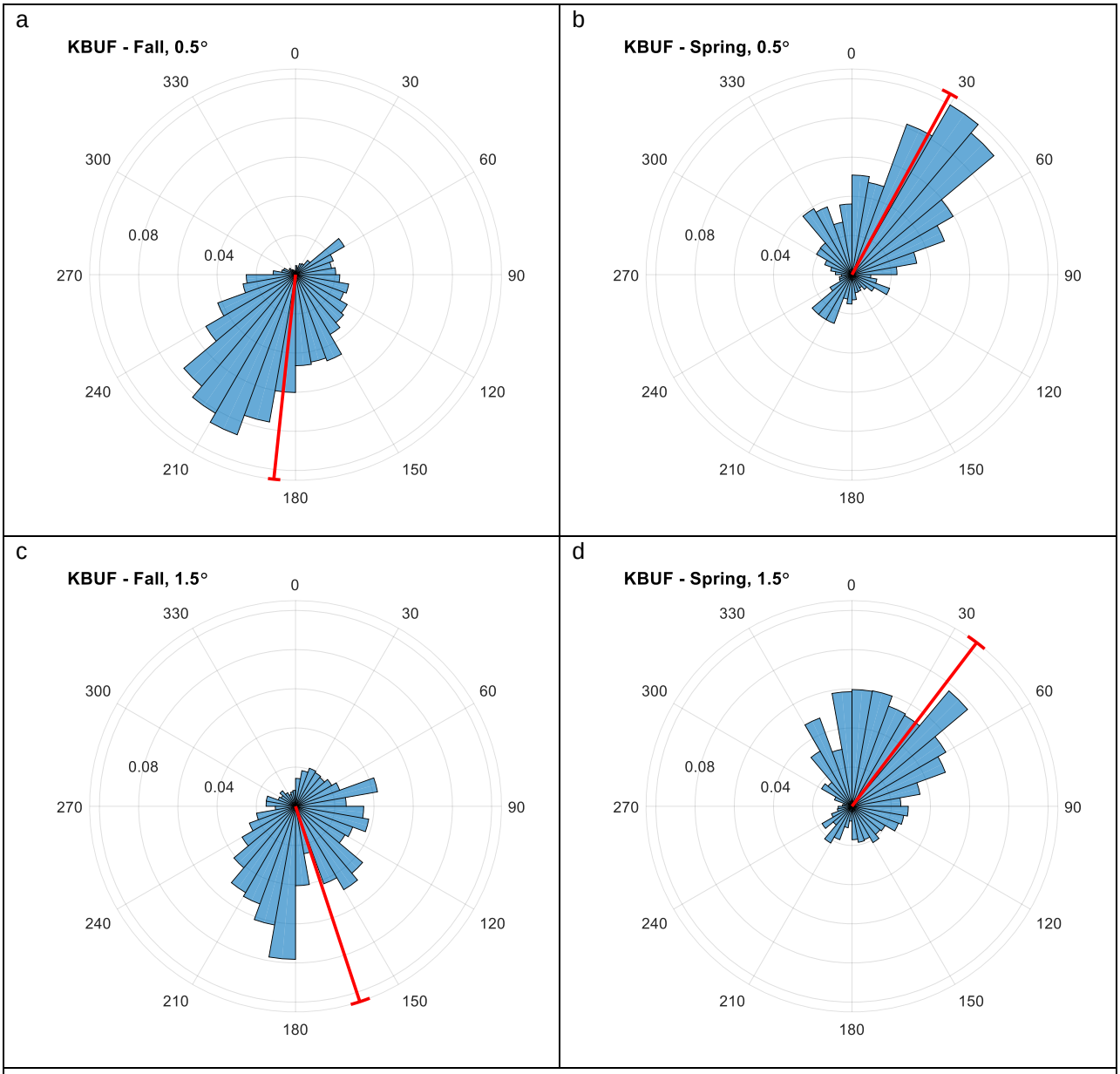

Figure 5. Rose plots showing target movement directions at KBUF at radar beam elevations of 0.5° (a and b) and 1.5° (c and d) in Fall (a and c) and Spring (b and d). Red lines indicate mean direction (radial segment) and 95% confidence interval (perpendicular "T" segment).

Table 4 provides statistical summaries (mean, concentration, and standard deviation) of direction by radar station, elevation, season, and year. For the most part, mean annual directions are consistent with the overall patterns in Figures 4 and 5. However, mean directions at KCLE in spring 2014 did not follow the expected pattern; that is, mean target headings were toward the southeast (154.5°) at the 0.5 degree elevation and toward the south-southwest (206.2°) at the 1.5 degree elevation. While there was also substantial variation in spring 2014 at KCLE; note that *r* was exceptionally low and, correspondingly, that *s* was high. More generally, target directions showed fairly high variability (low concentration); in most cases in Table 4, *r* was less than 0.5.

Table 4. Radar target direction summary: mean, concentration (*r*), and standard deviation (*s*) by station, season, year, and radar elevation.

			KCLE			KBUF		
Season	**Year**	**Elevation**	**Mean (°)**	***r***	***s* (°)**	**Mean (°)**	***r***	***s* (°)**
Spring	2014	0.5°	154.5	0.14	113.9	18.5	0.43	74.9
		1.5°	206.2	0.17	107.3	30.7	0.43	74.0
	2015	0.5°	14.1	0.41	76.3	43.3	0.54	63.7
		1.5°	14.9	0.40	77.3	49.1	0.46	71.7
	2016	0.5°	29.6	0.35	83.1	12.7	0.32	86.1
		1.5°	34.9	0.31	87.3	14.1	0.27	93.0
	All Years	0.5°	31.2	0.21	100.7	28.5	0.43	74.1
		1.5°	24.2	0.16	110.4	37.3	0.40	77.1
Fall	2013	0.5°	244.0	0.33	85.8	187.5	0.61	57.1
		1.5°	248.6	0.22	99.5	159.6	0.27	92.4
	2014	0.5°	219.2	0.49	68.4	199.5	0.68	50.5
		1.5°	217.1	0.38	79.6	175.3	0.36	82.3
	2015	0.5°	225.5	0.38	79.3	170.5	0.43	74.7
		1.5°	209.4	0.22	99.1	155.2	0.44	73.6
	All Years	0.5°	227.6	0.40	78.0	186.1	0.54	63.8
		1.5°	222.8	0.27	93.2	161.8	0.36	81.9

Migration Intensity

Migration intensity as represented by mean reflectivity varied among the seven sample areas at the two radar stations (Table 5, Figure 6). Overall mean reflectivity, averaged across season, year, and radar elevation, was lowest at the Project Area at KCLE (Figure 6a). Reflectivity was approximately twice as high at the two sample areas at KCLE overlapping the lakeshore (Comparison Areas 1 and 2) and somewhat greater at the inland sample area (Comparison Area 4). Mean reflectivity was highest at the two nearshore sample areas at KBUF (Comparison Areas 4 and 5), approximately eight times greater than mean reflectivity at the Project Area. At the inland KBUF sample area (Comparison Area 6), reflectivity was much lower than at the other two KBUF sample areas, though it was approximately 1.5 times greater than at the Project Area.

Table 5. Reflectivity by sample area (PA = Project Area, CA = Comparison Area). Each cell contains mean (top) and standard error (bottom) of reflectivity. (See also Figure 6.)

		KCLE				KBUF		
		PA	**CA1**	**CA2**	**CA3**	**CA4**	**CA5**	**CA6**
Overall		7.85 0.09	18.33 0.28	18.12 0.19	22.39 0.37	62.09 2.18	65.07 1.85	12.73 0.18
Elevation	0.5°	11.14 0.16	26.69 0.53	27.85 0.33	32.91 0.70	116.85 4.28	120.31 3.59	18.14 0.31
	1.5°	4.44 0.09	9.95 0.15	8.30 0.14	11.84 0.17	7.18 0.14	8.86 0.20	7.25 0.16
Season	Spring	6.44 0.13	16.13 0.58	16.11 0.28	20.63 0.76	65.71 3.66	56.14 2.64	6.89 0.15
	Fall	8.77 0.13	19.88 0.25	19.51 0.26	23.62 0.32	59.94 2.71	70.81 2.53	16.21 0.27
Year	2013 – 2014	6.02 0.12	15.55 0.33	14.42 0.29	19.22 0.47	116.69 5.38	103.15 4.36	13.07 0.29
	2014 – 2015	9.58 0.20	20.31 0.35	20.82 0.36	21.66 0.42	58.88 3.39	75.74 3.25	12.49 0.31
	2015 – 2016	8.05 0.16	19.21 0.68	19.23 0.34	26.16 0.87	8.25 0.22	15.55 0.59	12.63 0.34

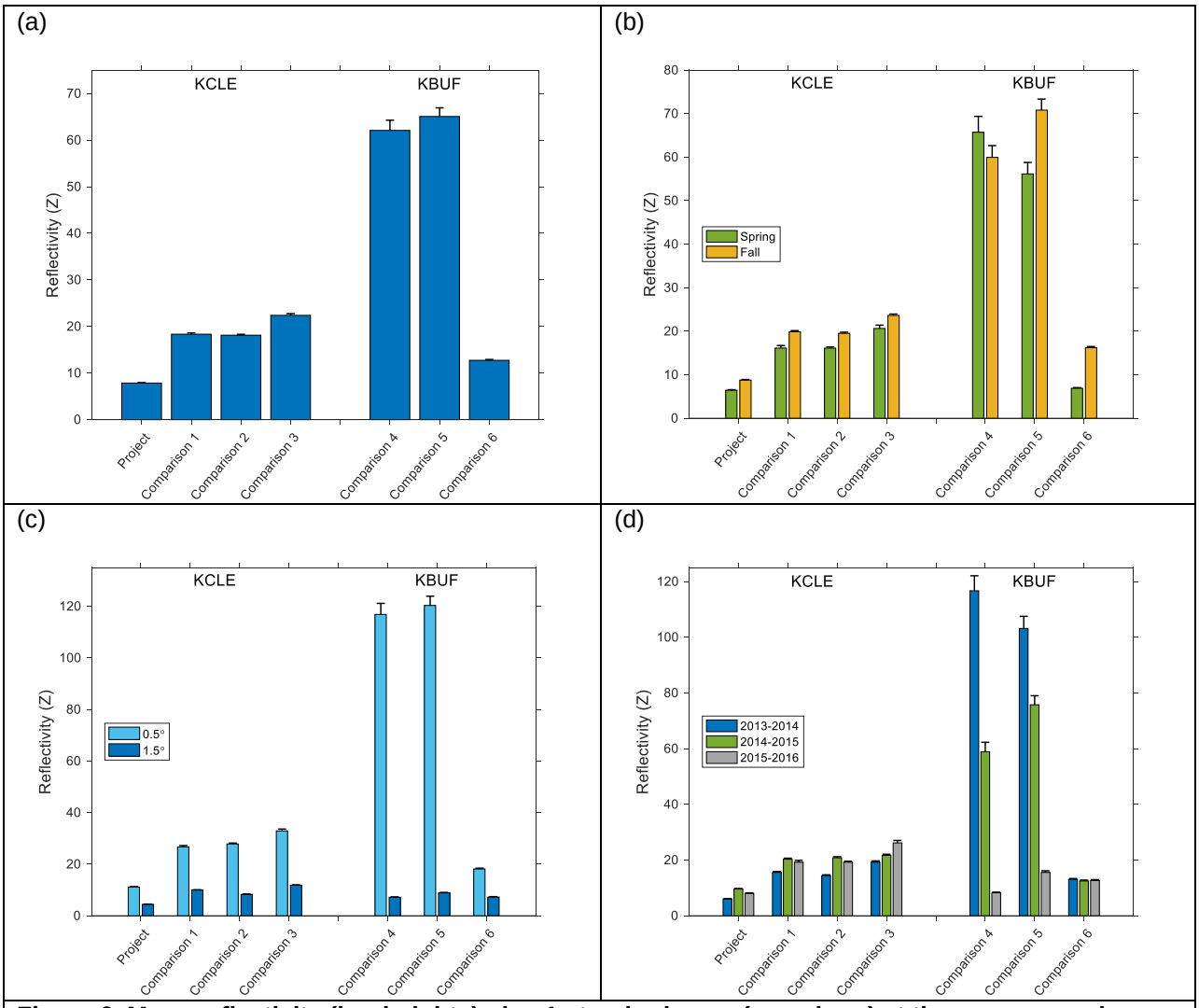

Figure 6. Mean reflectivity (bar heights) plus 1 standard error (error bars) at the seven sample areas:
(a) degrees overall – averaged across season, year, and elevation
(b) by season – averaged across year and elevation
(c) by elevation – averaged across season and year
(d) by year – averaged across season and elevation.

Reflectivity showed moderate seasonal variation at each of the sample areas, and was generally higher in the fall than in the spring, except at Comparison Area 4, where reflectivity was greater in the spring (Table 5, Figure 6b). For the seasonal analysis, reflectivity was averaged across year and radar elevation.

At each sample area there was substantial difference in mean reflectivity depending on radar elevation (reflectivity averaged across year and season) (Table 5, Figure 6c). In particular, reflectivity was at least twice as great at the 0.5 degree elevation as at the 1.5 degree elevation, though at Comparison Areas 4 and 5, the differences were particularly pronounced. That is, target densities were much greater at lower heights above the lake or land surface. In general,

the differences among the sample areas seen in Figure 6a are due to reflectivity differences at the lower radar elevation (Figure 6c). At the greater radar elevation, the differences in reflectivity among the sample areas are relatively small.

For most of the sample areas, there was little to moderate annual variation in mean reflectivity (averaged across season and radar elevation) (Table 5, Figure 6d). Here, a year was arbitrarily defined as a fall season and the succeeding spring season, e.g., fall 2013 through spring 2014, such that there were three years of data. Interestingly, the annual variation in reflectivity was substantial at Comparison Areas 4 and 5; it can be seen that the high overall reflectivity at these two areas was due to exceptionally high values in 2013-2014, and 2014-2015. In contrast, mean reflectivity in 2015-2016 at these two areas was similar to values at the other sample areas.

Mean reflectivity varied by time of night, as defined by an hour after civil sunset, at both KCLE and KBUF, in both fall and spring (Figure 7). At KCLE, reflectivity increased each hour until five hours after civil sunset, and thereafter decreased hourly in both seasons (Figure 7a, b). At KBUF, the hourly pattern varied with season. In the fall, there was little if any initial increase, though reflectivity decreased from four hours after civil sunset until daylight (Figure 7c). In the spring, reflectivity increased until about seven hours after civil sunset, changed little for the next few hours, and then decreased substantially in the last hour before daylight (Figure 7d).

Reflectivity varied substantially by date throughout each season (Figures 8-11). No clear patterns are evident in the fall (panel a in Figures 7-10). In the spring, there is little activity throughout April compared to May, particularly at the Project Area (Figure 8b) and Comparison Area 2 (Figure 9b).

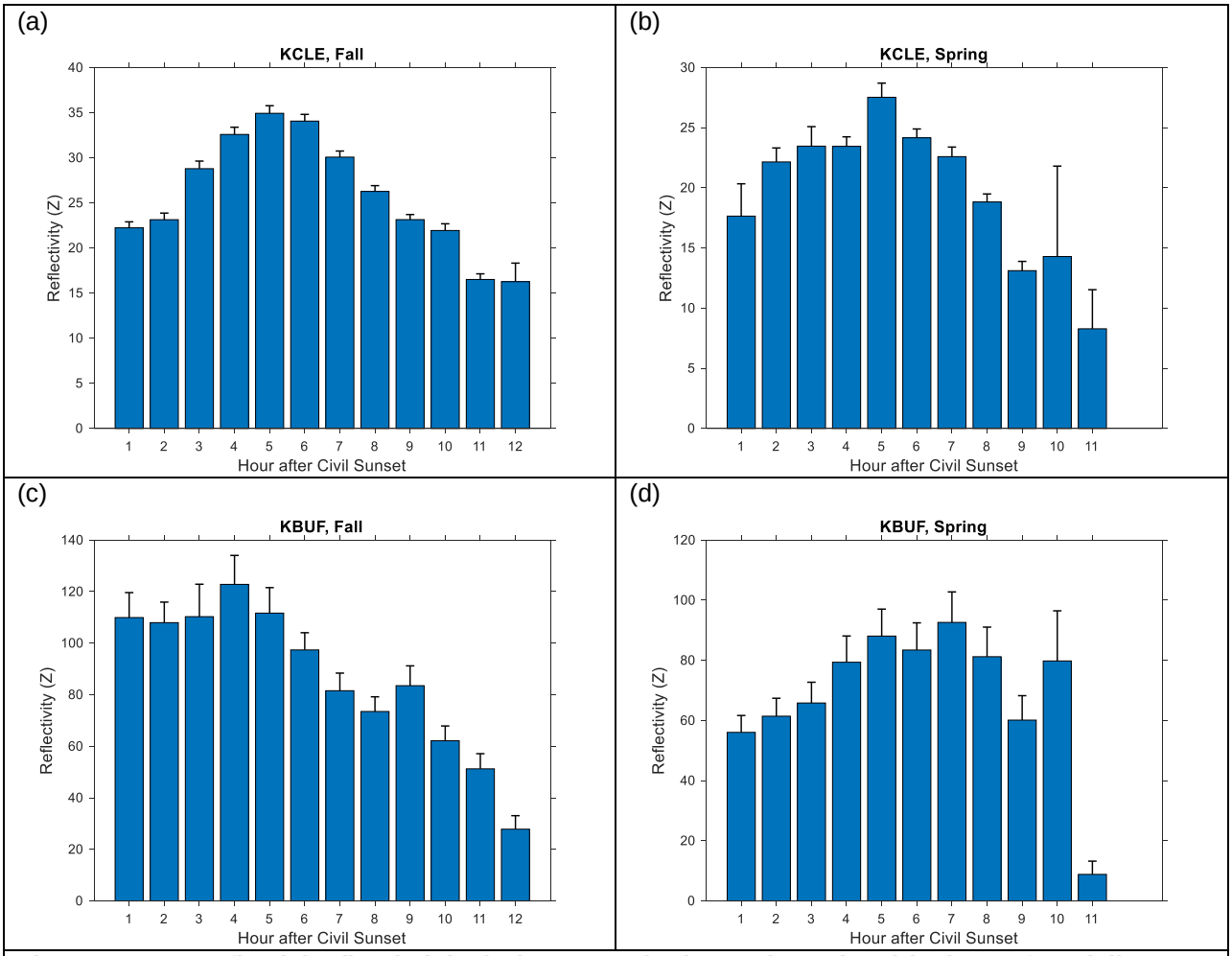

Figure 7. Mean reflectivity (bar heights) plus 1 standard error (error bars) by hour after civil sunset at KCLE and KBUF
(a) KCLE in fall
(b) KCLE in spring
(c) KBUF in fall
(d) KBUF in spring
All plots represent 0.5° elevation averaged across year and sample area. Note different Y-axis scaling in each plot.

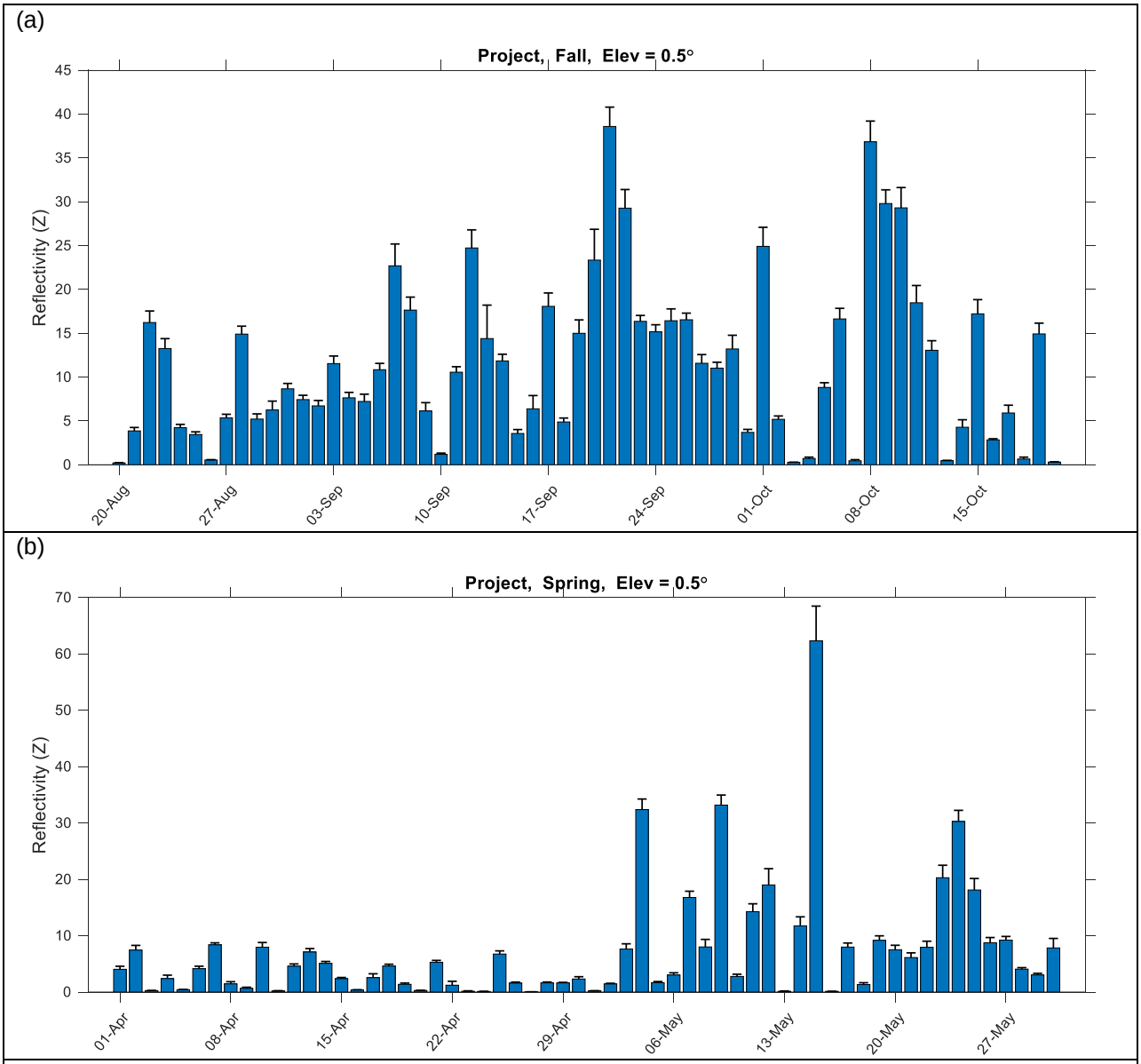

Figure 8. Mean reflectivity by day at the Project Area (KCLE) in (a) fall and (b) spring. Both plots represent 0.5° elevation averaged across year. Note different Y-axis scaling in each plot.

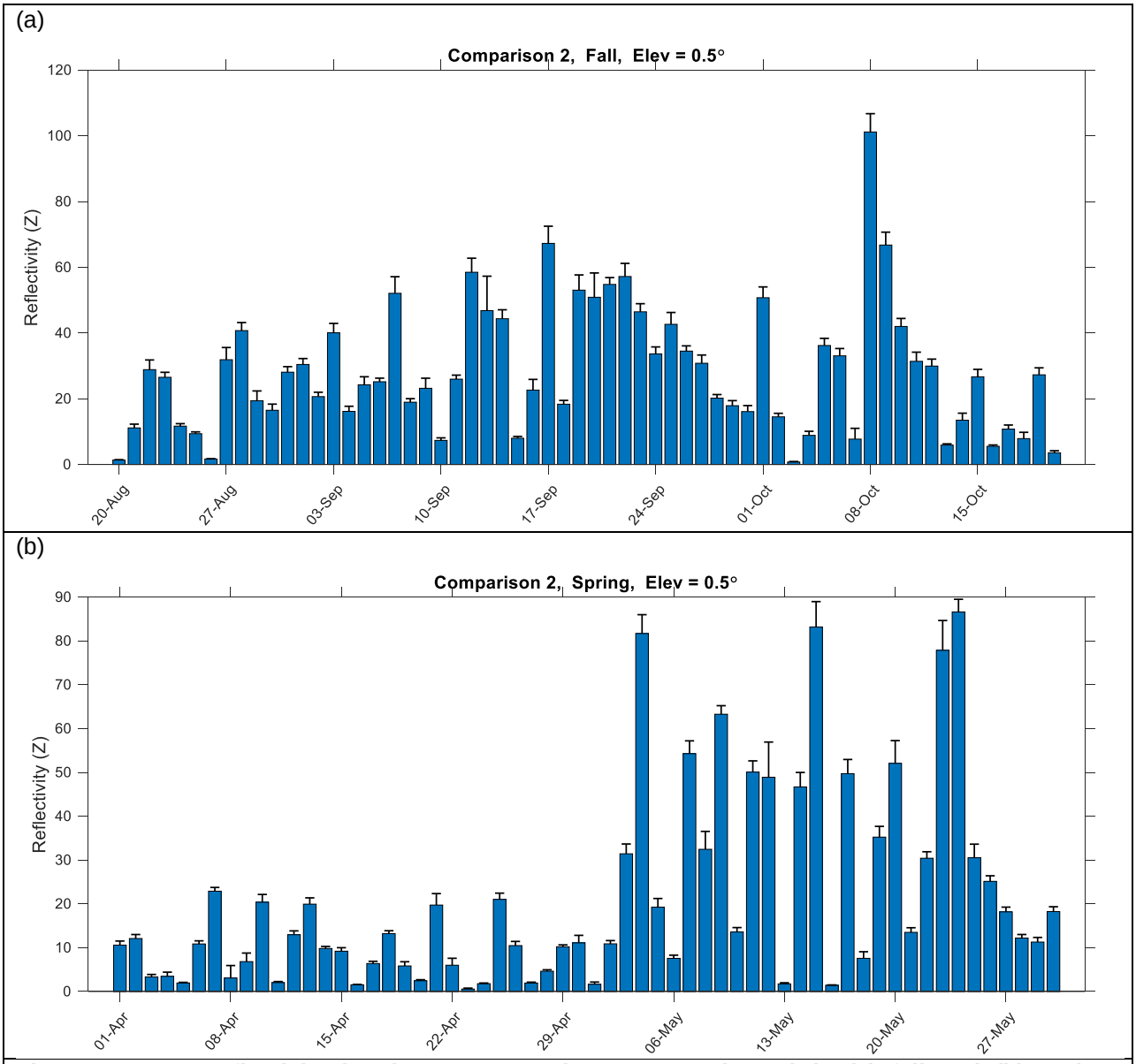

Figure 9. Mean reflectivity by day at Comparison Area 2 (KCLE) in (a) fall and (b) spring. Both plots represent 0.5° elevation averaged across year. Note different Y-axis scaling in each plot.

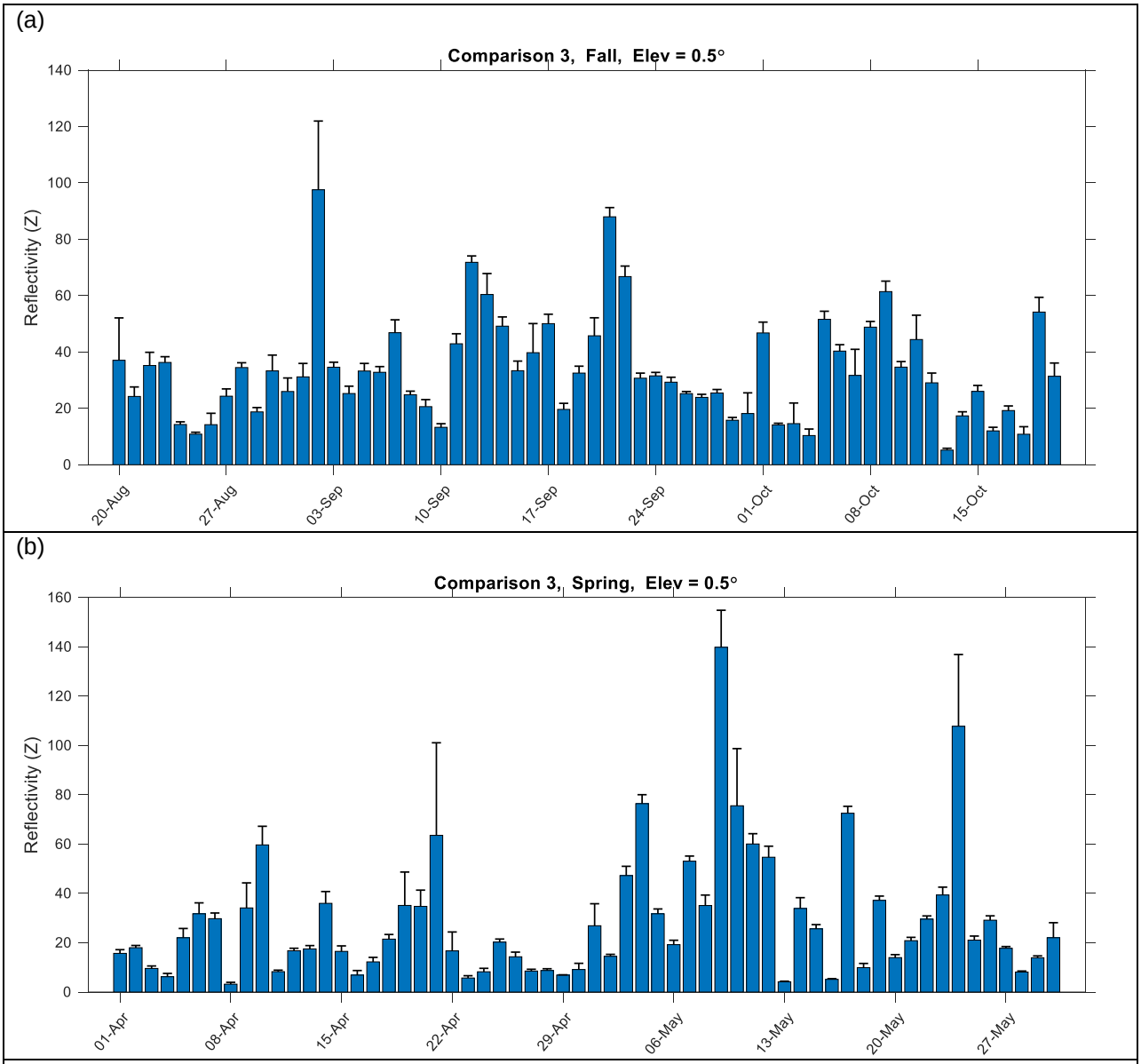

Figure 10. Mean reflectivity by day at Comparison Area 3 (KCLE) in (a) fall and (b) spring. Both plots represent 0.5° elevation averaged across year. Note different Y-axis scaling in each plot.

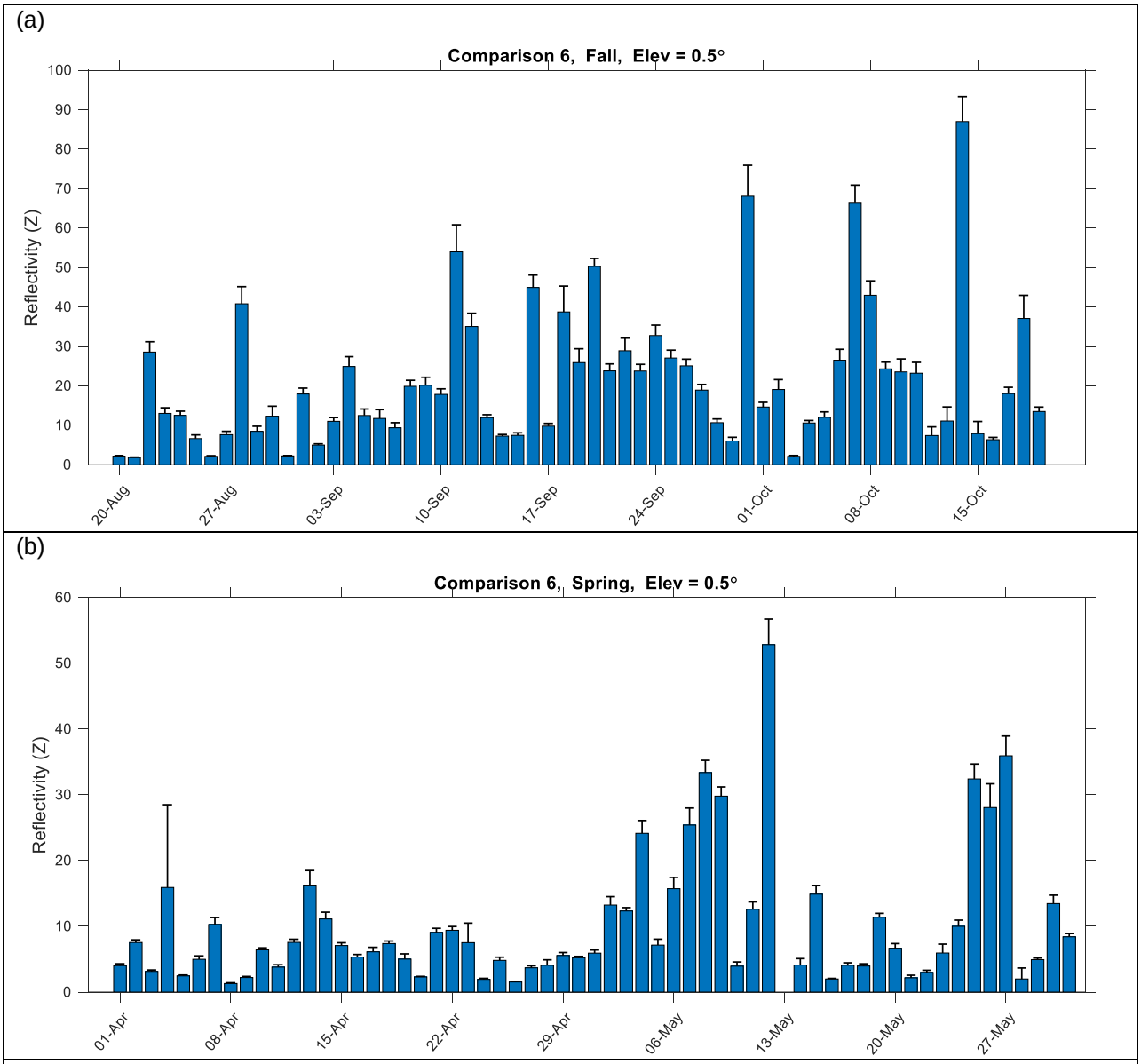

Figure 11. Mean reflectivity by day at Comparison Area 6 (KBUF) in (a) fall and (b) spring. Both plots represent 0.5° elevation averaged across year. Note different Y-axis scaling in each plot.

DISCUSSION

Caveats

The methods used here make at least two important assumptions. First, wind speed and direction from both radiosonde and wind models are assumed to be uniform over large spatial and temporal scales. That is, the wind is assumed to be constant over the region scanned by the radar for a relatively long period (up to 12 hours). Spatial and temporal variation in wind patterns will lead to errors in velocity filtering, which is intended to separate birds from slower-moving targets. Second, movement characteristics of radar targets (i.e., speed and direction) are treated as effectively uniform over large regions. Finer scale variation in target direction, velocity, or density will be obscured in this processing.

There are several other important limitations to this analysis. It cannot distinguish individual targets, nor can it distinguish birds from bats, nor any other target that might move faster than measured wind speed. Furthermore, the velocity filter is a fairly crude tool. For instance, slow-moving targets, such as birds soaring on the wind, will be automatically removed. Also, NEXRAD cannot detect targets that are close to the ground, except at very close range. In the case of KCLE, most near range data will necessarily be over land, or close to shore over Lake Erie.

Summary and Conclusion

Results from this analysis show that overall migration intensity inferred from mean reflectivity was lowest above the Project Area among all seven sample areas (Figure 6a). That relationship was also true when reflectivity was averaged by season (Figure 6b), radar elevation (Figure 6c), and year (Figure 6d). That is, migration intensity was lower at the Project Area than at all of the comparison sample areas in both spring and fall, at radar elevations of both 0.5 degrees and 1.5 degrees, and in all three years. Though, notably, migration at Comparison Area 6 in the spring was only slightly greater than at the Project Area in the same season (Figure 6b), and migration at Comparison Area 4 in 2015-2016 was only slightly greater than at the Project Area in the same year (Figure 6d).

At the KCLE station in Cleveland, the inland sample area, Comparison Area 3, had the greatest overall migration intensity, while the two areas above the shoreline, Comparison Areas 1 and 2, had migration that was intermediate to the inland and offshore areas (Figure 6a). Again, these patterns held true by season, radar elevation, and year (Figures 6b, 6c, 6d).

At the KBUF station in Buffalo, Comparison Areas 4 and 5, which were completely and partly above water, respectively, had much greater migration than any of the other sample areas (Figure 6). While this held true for both seasons, at the lower radar elevation, and for two of the three years of the study, it was not true at the 1.5 degree radar elevation nor in the last year (2015-2016). In those conditions, migration was generally greater in the other Comparison Areas. Thus, for the most part, the relative migration intensity at over-water and inland sites at KBUF was the reverse of the spatial pattern at KCLE. While the reason for these differences is not clear, it is noteworthy that Comparison Areas 4 and 5 at KBUF are situated at a very narrow

section of Lake Erie at the eastern end of the Lake. Comparison Area 4 is entirely above water, but close to land on three sides (Figure 2b). The distance from south to north shore at this narrow end of the lake is less than 10 km.

Livingston (2008) conducted a study at KCLE for the proposed Icebreaker Wind Energy Facility. The methods in that earlier study differed from those of the current study in that the earlier study focused on a single sample area above the proposed project and, for that area, used data from the 0.5 degree radar elevation only. No other sample areas at that elevation were examined. Data from the 1.5 degree radar elevation were analyzed, though that analysis included the entire radar sweep, that is, a much larger area over both water and land. Thus, unambiguous comparisons of migration intensities over land and water, and, similarly, comparisons of migration intensities at the two radar elevations are difficult with the Livingston (2008) analysis. That said, the range of migration intensities over both seasons is comparable to values in this study. For instance, if bird densities in the upper panels of Figures 4 and 5 of Livingston (2008) are back-converted to reflectivity (*Z*), then it can be seen that on most nights of both spring and fall, mean reflectivity was less than 20 *Z*. Furthermore, on most of the remaining nights, mean reflectivity was in the range 20-40 *Z*. Those results are consistent with nightly variation seen in this study (Figure 8). Also, as in this study, fall migration intensity was generally greater than spring in Livingston (2008) (compare the upper panels of Figure 4 and 5, spring and fall, respectively, in Livingston, 2008).

Diehl et al. (2003) analyzed bird migration in the Great Lakes region using NEXRAD data from three stations (including KCLE and KBUF), and found that bird densities over land were generally greater than over water, consistent with results from KCLE in this study (Table 5 and Figure 6). Diehl et al. (2003) attributed this pattern in relative migration density to lake avoidance. That is, while large numbers of birds flew over the Great Lakes, even larger numbers remained over land during migration in both seasons.

Such avoidance behavior might account for the particularly high migration intensities seen at KBUF in two of the three years of this study. Bird migrating around the east end of Lake Erie might have chosen to cross this narrow section of water where land was nearby in three directions. Notably, while Diehl et al. found higher densities over land than over Lake Erie at both KBUF and KCLE, the difference at KBUF was small and not statistically significant.

In comparing seasonal patterns of migration, Diehl et al. observed that fall densities at KBUF were greater than spring densities over both land and water, though at KCLE densities were greater in spring than in fall. In this longer, three-year study, densities were generally greater in the fall than in the spring at both stations, though these seasonal differences were generally small (Figure 6b).

Results from this study suggest that bird/turbine collision risk for the proposed offshore project is lower than it would be for a similar project located near shore or onshore in the Cleveland area. Furthermore, based on variation in migration intensity, annual variation in risk and seasonal variation, with somewhat higher risk in fall, would be expected. Differences in migration intensity with radar elevation indicate that, at the Project Area, there are more than twice as many birds at the lower 0.5 degree elevation (Figure 6c). While the airspace sampled at this elevation does

overlap with the rotor-swept zone, the extent of overlap is small (Figure 3), thus the migrant bird activity detected by this lower beam primarily comes from altitudes immediately above the rotor swept zone of the turbines. Given the limitations of NEXRAD resolution, it is not possible to determine the precise flight altitudes of birds within the radar beam.

REFERENCES

Archibald, K.M., J.J. Buler, J.A. Smolinsky, and R.J. Smith. 2016. Migrating birds reorient toward land at dawn over the Great Lakes, USA. *Auk* 134:193-201.

Batschelet, E. 1981. *Circular Statistics in Biology*. Academic Press, London.

Bonter, D.N., S.A. Gauthreaux, Jr., and T.M. Donovan. 2008. Characteristics of important stopover locations for migrating birds: remote sensing with radar in the Great Lakes Basin. *Conservation Biology* 23:440-448.

Buler, J.J. and D.K. Dawson. 2014. Radar analysis of fall bird migration stopover sites in the northeastern U.S. *Condor* 116:357-370.

Browning, K.A. and R. Wexler. 1968. The determination of kinematic properties of a wind field using Doppler radar. *Journal of Applied Meteorology* 7:105-113.

Chilson, P.B. and E.M. Adams. 2014. Utility of WSR-88 weather radar for monitoring nocturnal avian migration in the offshore environment. In: *Wildlife Studies on the Mid-Atlantic Continental Shelf*, Biodiversity Research Institute 2014 Annual Report.

Chilson, P.B., W.F. Frick, P.M. Stepanian, J.R. Shipley, T.H. Kunz, and J.F. Kelly. 2012. Estimating animal densities in the aerosphere using weather radar: to Z or not to Z? *Ecosphere* 3(8), Article 72.

Diehl, R.H. and R.P. Larkin. 2005. Introduction to the WSR-88D (NEXRAD) for ornithological research. USDA Forest Service Gen. Tech. Rep. PSW-GTR-191, pp. 876-888.

Diehl, R.H. R.P. Larkin, and J.E. Black. 2003. Radar observations of bird migration over the Great Lakes. *Auk* 120:278-290.

Doviak, R.J. and D.S. Zrnic. 2006. *Doppler Radar and Weather Observations*, 2nd ed. Dover Publications, Mineola, NY.

Farnsworth, A., B.M. Van Doren, W.M. Hochachka, D. Sheldon, K. Winner, J. Irvine, J. Geevarghese, and S. Kelling. 2016. A characterization of autumn nocturnal migration detected by weather surveillance radars in the northeastern USA. *Ecological Applications* 26:752-770.

Gauthreaux, S.A. and C.G. Belser. 1998. Displays of bird movements on the WSR-88D: patterns and quantification. *Weather and Forecasting* 13:453-464.

Gauthreaux, S.A. and C.G. Belser. 2003. Radar ornithology and biological conservation. Auk 120:266-277.

Liang, X. and B. Wang. 2009. An integrating VAP method for single-doppler radar wind retrieval. *Acta Meteorologica Sinica* 23:166-174.

Livingston, J.W. 2008. Analysis of WSR-88D Data to Assess Nocturnal Bird Migration Offshore of Cleveland, Ohio. Prepared by Geo-Marine, Inc. for Curry & Kerlinger, LLC.

Manly, B.F.J. 2006. *Randomization, Bootstrap and Monte Carlo Methods in Biology*, 3rd ed. Chapman and Hall/CRC, Boca Raton.

Mardia, K.V. 1972. *Statistics of Directional Data*. Academic Press, New York.

North American Datum (NAD). 1983. Nad83 Geodetic Datum.

NOAA. 2016. *WSR-88D Meteorological Observations, Federal Meteorological Handbook No. 11*. National Oceanic and Atmospheric Administration, U.S. Department of Commerce.

Raghavan, S. 2013. *Radar Meteorology*. Springer Netherlands.

Torres, S.M. and C.D. Curtis. 2007. Initial implementation of super-resolution data on the NEXRAD network. 23rd Conference on Interactive Information Processing Systems, American Meteorological Society.